FCH JU Grant Agreement no.:	245228
Project acronym:	PrimoLyzer
Project title:	Pressurized PEM Electrolyser Stack
Funding scheme:	
Area:	SP1-JTI-FCH.2.1: Efficient PEM Electrolysers SP1-JTI-FCH.3.2: Component and system improvement for stationary applications
Start date of project:	01.01.2010
Duration:	24 months
Project Coordinator:	IRD Fuel Cells A/S

Deliverable Report:

Report on modelling of $IrRuMO_x$ catalysts completed

(D 2.4)

Author (partner):	Dr. Pertti Kauranen (VTT)
Other authors:	Dr. Eini Puhakka (VTT)
Work package:	WP2
Work package leader (partner):	Dr. Pertti Kauranen (VTT)
Date released by WP leader:	Monday, 02 January 2012
Date released by Coordinator:	Monday, 02 January 2012

Dissemination level		
PU	**Public**	**X**
PP	**Restricted to other programme participants (including the Commission Services)**	
RE	**Restricted to a group specified by the consortium (including the Commission Services)**	
CO	**Confidential, only for members of the consortium (including the Commission Services)**	

Revisions			
Version:	Date:	Changed by:	Comments:
1st draft	28 April 2011		
2nd draft	23 June 2011	E. Puhakka	
3rd draft	3 October 2011	E. Puhakka	
4th draft	25 November 2011	E. Puhakka	
5th draft	22 December 2011	P. Kauranen	
6th final	02 January 2012	L. Grahl-Madsen	Changed the dissemination level to public

Deliverable Report:
Report on modelling of $IrRuMO_x$ catalysts completed
(D 2.4)

1. Introduction

The aim of the study was to define the oxygen evolution reaction (OER) mechanism on the surfaces of binary and tertiary metal oxides, e.g. $IrRuO_4$, $IrRuSnO_x$ or $IrRuTaO_x$. The auspicious catalyst composition was optimized by combining theoretical quantum mechanical calculations of mixed oxide crystal and surface structures and their interactions with water and oxygen as well as experimental work.

The crystal and surface structures of catalysts were investigated using density functional methods. The investigated catalysts consisted of pure metal oxides (IrO_2, RuO_2 and SnO_2) with rutile structure, and binary (Ir_7RuO_{16} and $RuIrO_4$) and tertiary metal oxides (Ir_2RuSnO_8) with rutile-like structures.

2. Calculation methods

All the calculations were performed with the CASTEP (Cambridge Serial Total Energy Package) code implemented into Materials Studio version 5.0 (Accelrys, 2009). In these calculations, the total electronic energy and overall electronic density distribution were solved in order to define the energetically stable surface structures and surfaces with reagents.

During the geometry optimization of the crystal and surface structures of catalysts, and reaction mechanism studies, the exchange-correlation was described with generalized gradient approximation GGA-PBE. As a compromise between the accuracy and computational time of calculations, the ultrasoft pseudopotentials were used for each element. The used potentials were H_00PBE.usp for hydrogen, Ir_00PBE.usp for iridium, O_soft00.usp for oxygen, Ru_00PBE.usp for ruthenium, and Sn_00PBE.usp for tin. The kinetic cut-off energy for a plane wave expansion of the wave function was 280 eV.

3. Earlier modelling studies

In literature, there are some molecular modelling studies where the OER mechanism has been investigated on metal (Pt, Au) and metal oxide (RuO_2) surfaces (Rossmeisl et al., 2005; Rossmeisl et al., 2007). Rossmeissl et al. (Rossmeisl et al., 2007) calculated the OER reaction on oxygen atom or hydroxide covered RuO_2 surface at low overpotentials using the following path, where the * represents active site on the metal surface (Scheme 1):

$2\ H_2O \rightarrow HO^* + H_2O + H^+ + e^-$ (1)

$\rightarrow O^* + H_2O + 2\ H^+ + 2\ e^-$ (2)

$\rightarrow HOO^* + 3\ H^+ + 3\ e^-$ (3)

$\rightarrow O_2 + 4\ H^+ + 4\ e^-$ (4)

In these studies the reaction mechanism has been fixed and only the reaction intermediates and energetics of these steps have been calculated, but transition states between the intermediates have not been determined in order to verify the reaction path. Moreover, the method was not applied to mixed metal oxide surfaces.

4. Crystal structures and lattice parameters

Of planar surface structures of different oxide catalysts, the (001) surface was selected for OER studies. The (001) surfaces of the different Ir-Ru mixed oxides are given in Figure 1. It should be noted that Ir_7RuO_{16} has an Ir rich surface layer and is expected to behave close to pure IrO_2. $RuIrO_4$ has Ru rich surface layer and is expected to behave more like RuO_2.

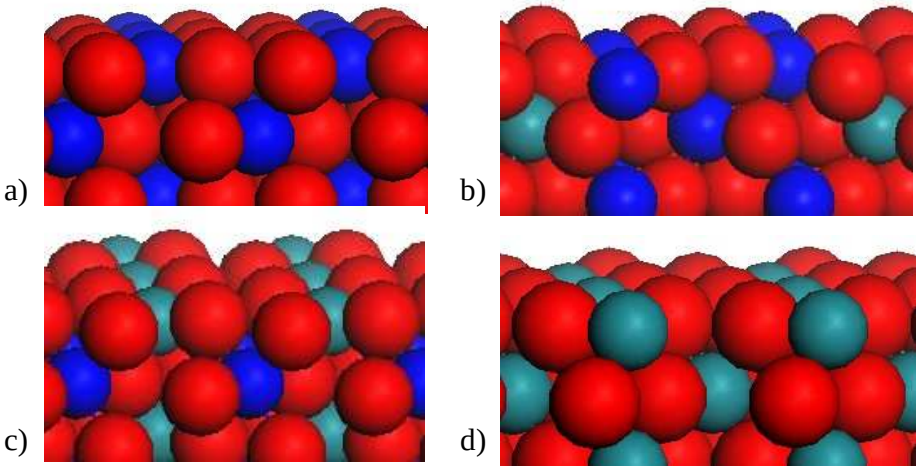

Figure 1. The (001) surface of a) IrO_2, b) Ir_7RuO_{16}, c) $RuIrO_4$, and d) RuO_2. Blue spheres: iridium. Red spheres: oxygen. Turquoise spheres: ruthenium.

The lattice parameters of different pure and mixed binary rutile type oxides are given in Table 1.

Table 1. Lattice parameters for rutile type of oxides.

	a		b		c	
	Exptl. (Å)	Calc. (Å)	Exptl. (Å)	Calc. (Å)	Exptl. (Å)	Calc. (Å)
IrO_2	4.498	4.651	4.498	4.651	3.155	3.241
RuO_2	4.492	4.532	4.492	4.532	3.107	3.120
$IrRuO_4$		4.582		4.582		3.176
Ir_7TaO_{16}		9.381		9.381		3.251
Ir_7RuO_{16}		9.260		9.260		3.229
Ir_3RuO_8		9.208		4.630		3.207
$IrRu_3O_8$		9.138		4.537		3.154
$IrRu_7O_{16}$		9.071		9.071		3.140
Ir_2RuSnO_8		9.361		4.679		3.221
MnO_2	4.390	4.516	4.390	4.516	2.860	2.832
SnO_2	4.737	4.916	4.737	4.916	3.186	3.273
TaO_2	13.320	14.412	13.320	14.412	6.120	6.147
NbO_2	13.702	13.792	13.702	13.792	5.982	6.015

In order to have a more even surface atom distribution and better correspondence to nanostructured catalysts, the stepped (101) surface and its multiple plane (201) were calculated for $RuIrO_4$ and the tertiary Ir_2RuSnO_8, Figure 2.

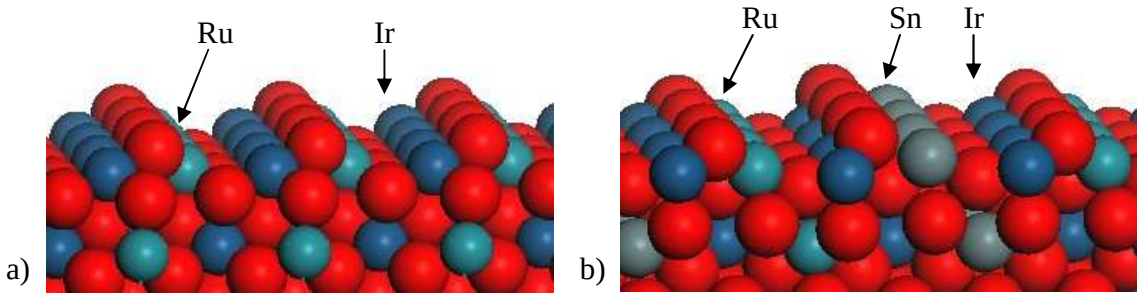

Figure 2. a) The (101) surface of $RuIrO_4$, and b) the (201) surfaces of Ir_2RuSnO_8.

5. Reaction mechanism

The OER reaction mechanism was first derived for the neutral IrO_2 surface and then a positive surface charge was introduced in order to account for the electrochemical potential. Unlike in the previous studies (Rossmeisl et al., 2005; Rossmeisl et al., 2007), the surface was assumed initially adsorbate free. Different reaction paths on the (001), (101) and (201) catalyst surfaces where the surface metal atoms are four-coordinated were calculated. Based on our studies, the most presumable total reaction is

$$5\ H_2O \rightarrow 2\ S\text{-}OH + 2\ S\text{-}H + \mathbf{4\ H^+ + 4\ e^- + O_2} + H_2O$$

where four water molecules dissociate, and then four protons desorb as H_3O^+ ions and oxygen as a molecule from the surface (Scheme 2). The calculated reaction steps were

$$5\ H_2O \rightarrow 4\ S\text{-}OH + 4\ S\text{-}H + H_2O \quad (1)$$

$$\rightarrow \underline{3\ S\text{-}OH} + S\text{-}O^- + 4\ S\text{-}H + \mathbf{H_3O^+} \quad (2)$$

$$3\ S\text{-}OH + S\text{-}O^- + 4\ S\text{-}H + H_2O \rightarrow 3\ S\text{-}OH + S\text{-}O^- + \underline{3\ S\text{-}H} + \mathbf{H_3O^+} + e^- \quad (3)$$

$$3\ S\text{-}OH + S\text{-}O^- + 3\ S\text{-}H + H_2O + e^- \rightarrow \underline{2\ S\text{-}OH} + 2\ S\text{-}O^- + 3\ S\text{-}H + \mathbf{H_3O^+} + e^- \quad (4)$$

$$2\ S\text{-}OH + \underline{2\ S\text{-}O^-} + 3\ S\text{-}H + H_2O + e^- \rightarrow 2\ S\text{-}OH + S\text{-}O_2 + 3\ S\text{-}H + H_2O + 3\ e^- \quad (5)$$

$$\rightarrow 2\ S\text{-}OH + \mathbf{O_2} + 3\ S\text{-}H + H_2O + 3\ e^- \quad (6)$$

$$2\ S\text{-}OH + 3\ S\text{-}H + H_2O + 3\ e^- \rightarrow 2\ S\text{-}OH + \underline{2\ S\text{-}H} + \mathbf{H_3O^+} + 4\ e^- \quad (7)$$

During the determination of this reaction mechanism, all the compounds on the surface were allowed to fully relax in order to find out interactions between different chemical groups. Comparison of the present OER to the reaction presented in Scheme 1 indicates that the present mechanism differs from the earlier determined mechanism by having surface oxygen molecule $S\text{-}O_2$ as a transition state instead of the surface peroxide HOO* intermediate product although the calculation could have produced this intermediate, too. According to Rossmeisl et al. (Rossmeisl et al., 2007) formation of the surface oxygen molecule is energetically unfavourable and was omitted in their calculation. The peroxide path

has also been proposed for oxygen evolution intermediate in alkaline media (Bockris, 1956). The details of the Scheme 2 are shown in Figure 3 for the positively charged (001) surface of IrO_2.

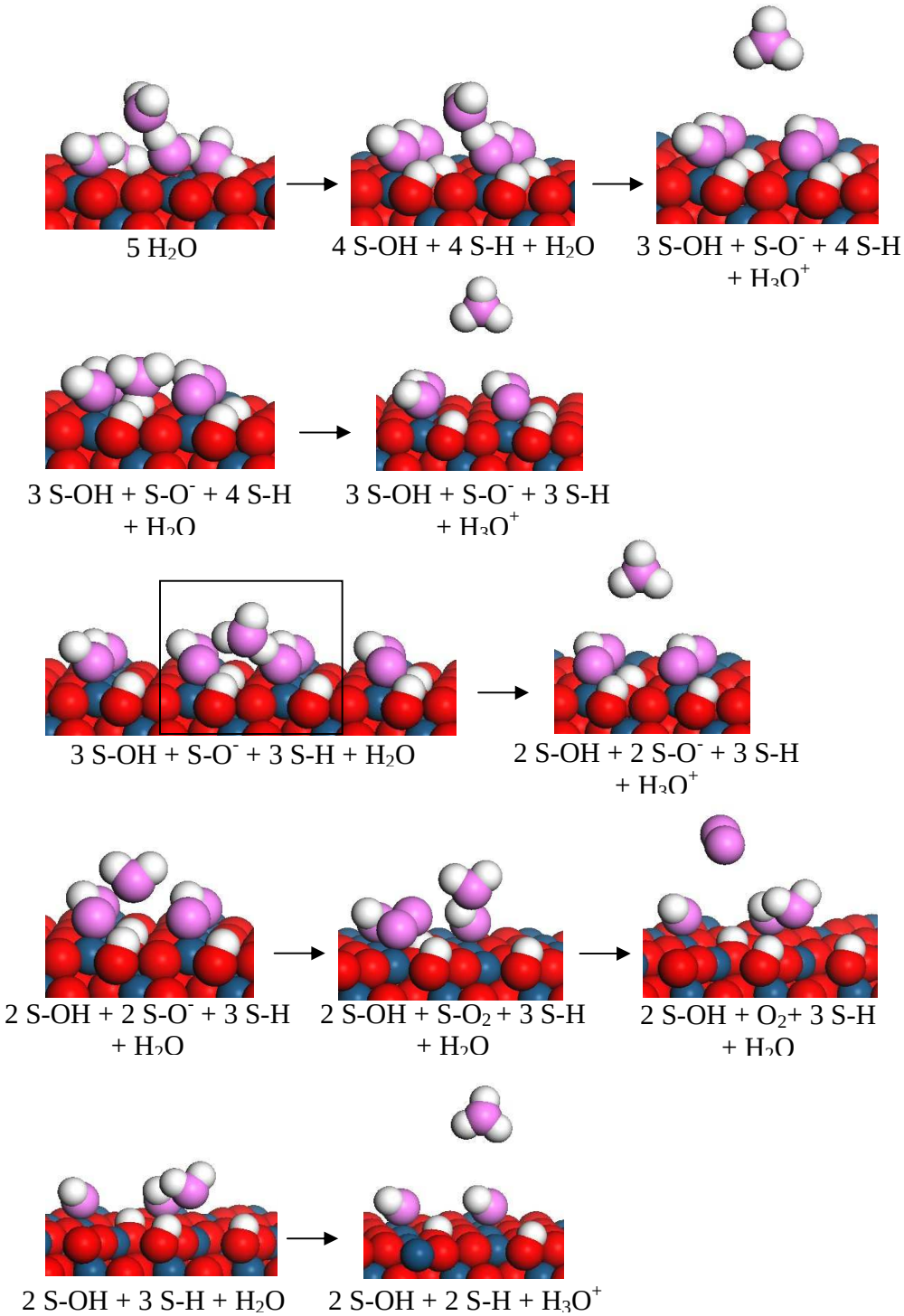

Figure 3. The reaction steps of the OER on the (001) surface of IrO_2.

6. Energetics on the (001) surface

According to Scheme 2, four protons as H_3O^+ ions desorbs from the surface. Because the desorbed protons of Steps 2-4 are not included into the calculations of the next steps, there is a need for an additional positive charge +3 during the reaction in order to keep the model system at the zero level charge. It should be noted that the last proton discharges in Step 7 remains in the system and does not need the charge balancing. Because these sub reactions of the OER happen on the anode, which is charged positively by external potential, the initial state for the calculations has been chosen so that the charge of the total OER does not reach negative values. Therefore, it was supposed that the total charge of the system is set up +3 in the beginning of the reaction, and after the desorption of protons, the system reaches the zero level charge. The energetics of the reaction steps are presented for Ir_7RuO_{16} and IrO_2 in Table 2.

Table 2. Energetics of OER (eV) on the (001) surfaces of Ir_7RuO_{16} and IrO_2.

			Ir_7RuO_{16}			**IrO_2**		
	Charge	Desorption	Barrier (eV)	Slope (eV)	Total (eV)	Barrier (eV)	Slope (eV)	Total (eV)
Step 1	3		1.41	-1.12	0.29	1.15	-1.08	0.07
Step 2	3	H^+	0.74	-0.06	0.67	0.77	-0.02	0.75
Step 3	2	H^+	1.56	0.35	1.91	1.62	0.34	1.96
Step 4	1	H^+	2.18	0.51	2.69	2.43	0.53	2.96
Step 5	0		4.26	-2.60	1.66	4.27	-2.71	1.56
Step 6	0	O_2	2.43	-0.05	2.38	2.34	-0.09	2.25
Step 7	0	H^+	5.07	-1.07	4.00	4.90	-1.19	3.71
					13.60			13.26

Comparison of the results indicates that the energetics of OER is very similar on the Ir_7RuO_{16} and IrO_2 surfaces. The most presumable reason for this is that the uppermost layer consists of Ir and O oxygen in the both cases (Figure 1a and 1b), and the effect of Ru atoms does not appear on this surface. The rate determining step (RDS) is the Step 5 (formation of the surface oxygen molecules) or the Step 7 (discharge of the last proton). However, the last reaction step (Step 7) was only calculated in order to obtain the total reaction energy for the stoichiometric reaction. In a real case where excess water is available, this step can be disregarded and Step 5 remains as the RDS. As previously mentioned the formation of the surface oxygen molecule is energetically unfavourable and has been omitted in the previous literature references. However, our approach produces this intermediate, not the peroxide HOO*.

In electrochemical evolution of oxygen, the anode is positively charged by the external potential. Based on this, it can be supposed that the charges of the sub reactions in Scheme 2 have only minor effect on the potential of the anode. Therefore, calculations with different positive values, from +1 to +4 were performed, and +3 was selected for the fixed total charge of the system in order to keep constant conditions for all the sub reactions.

The energetics of the OER for the (001) surfaces of IrO_2, $RuIrO_4$ and RuO_2 is presented in Table 3. The calculated reaction paths on the IrO_2, $RuIrO_4$ and RuO_2 surfaces are all according to the Scheme 2, Figure 3.

Table 3. Energetics (eV) of the OER on the (001) surfaces of IrO_2, $RuIrO_4$ and RuO_2.

	IrO_2			**$RuIrO_4$**			**RuO_2**		
	Barrier	Slope	Total	Barrier	Slope	Total	Barrier	Slope	Total
Step 1	1.15	-1.08	0.07	0.87	-0.20	0.67	2.25	-0.03	2.22
Step 2	0.77	-0.02	0.75	0.48	-0.09	0.39	0.57	-0.16	0.41
Step 3	0.74	-0.21	0.53	0.65	-0.34	0.31	0.53	-0.50	0.03
Step 4	0.59	-0.05	0.54	0.65	-0.10	0.55	0.53	-0.15	0.38
Step 5	4.29	-3.23	1.06	4.55	-3.11	1.44	4.73	-2.72	2.01
Step 6	1.87	-0.40	1.47	2.17	-1.19	0.98	2.48	-1.14	1.34
Step 7	4.59	-4.45	0.14	5.39	-4.58	0.81	5.06	-4.60	0.46
			4.56			5.15			6.85

The effect of the surface charge on the IrO_2 (001) surface are shown as decrease in the proton discharge energies (Steps 3 and 4) and desorption of the oxygen molecule (Step 6). However, the water dissociation energy (Step 1) and oxygen molecule formation (Step 5) which are chemical steps remain unchanged, compare Tables 2 and 3. It is interesting to note that positive discharge energies are still needed for the proton discharge from a positively charged surface.

Comparison of the energetics of the sub reactions in Table 3 indicates that each catalyst (Ir-Ru) has its own strength. The dissociation of water occurs most likely on the IrO_2 surface (Step 1), the desorption of protons is easier from the $RuIrO_4$ and RuO_2 surfaces than from the IrO_2 surfaces (Steps 2-4), and the formation and desorption of oxygen is more favourable on the IrO_2 surfaces than on the corresponding $RuIrO_4$ and RuO_2 surfaces (Steps 5-6). The rate-determining step (RDS) of the reaction is again the formation of oxygen molecule on the surface (Step 5). IrO_2 appears to be the most favourable surface for this reaction.

The synergetic effect of the $RuIrO_4$ is not fully shown in the values of Table 3 for the surface layer consists of Ru and O only, see Figure 1c. The results would be slightly different, if the uppermost layer had consisted of Ir and O atoms instead of Ru and O atoms. The total energies (4.6–6.9 eV) of the reactions are in the same order of magnitude as the free energies (about 5 eV) of the reactions according to Scheme 1.

7. Tin oxide

The same total OER was also calculated on the (001) surface of SnO_2. It was realized that the reaction mechanism differed slightly from those of the earlier investigated catalysts. In this reaction path, four protons desorb before the formation and desorption of an oxygen molecule (Scheme 3).

$5\ H_2O$	$\rightarrow 2\ S\text{-}OH + 2\ S\text{-}H + 3\ H_2O$	(1)
	$\rightarrow 3\ S\text{-}OH + 2\ S\text{-}H + H_2O + \mathbf{H_3O^+} + e^-$	(2)
$3\ S\text{-}OH + 2\ S\text{-}H + 2\ H_2O + e^-$	$\rightarrow 4\ S\text{-}OH + 2\ S\text{-}H + \mathbf{H_3O^+} + 2\ e^-$	(3)
$4\ S\text{-}OH + 2\ S\text{-}H + H_2O + 2\ e^-$	$\rightarrow 3\ S\text{-}OH + S\text{-}O^- + 2\ S\text{-}H + \mathbf{H_3O^+} + 2\ e^-$	(4)
$3\ S\text{-}OH + S\text{-}O^- + 2\ S\text{-}H + H_2O + 2\ e^-$	$\rightarrow 2\ S\text{-}OH + 2\ S\text{-}O^- + 2\ S\text{-}H + \mathbf{H_3O^+} + 2\ e^-$	(5)
$2\ S\text{-}OH + 2\ S\text{-}O^- + 2\ S\text{-}H + H_2O + 2\ e^-$	$\rightarrow 2\ S\text{-}OH + S\text{-}O_2 + 2\ S\text{-}H + H_2O + 4\ e^-$	(6)
	$\rightarrow 2\ S\text{-}OH + \mathbf{O_2} + 2\ S\text{-}H + H_2O + 4\ e^-$	(7)

Because the reaction path differs from the earlier defined path for Ir-Ru oxide catalyst, the results also depend on the our selection for the constant conditions for calculations. The energetics of this reaction mechanism is presented in Table 4, and the calculated reaction paths in Figure 4. The dissociation of water is spontaneous reaction on the SnO_2 surface. The desorption of protons demands more energy than on the (001) surfaces of IrO_2, $RuIrO_4$ and RuO_2 (Steps 2-5), but the formation and desorption of oxygen is exothermic reaction in contrast to the IrO_2, $RuIrO_4$ and RuO_2 (Steps 5-6). One of the reasons for the exothermal oxygen formation and desorption energies is Step 6, where two oxygen atoms form a trioxygen molecule with a surface oxygen atom as an intermediate product (Figure 5). The trioxygen intermediate appears unrealistic and could be considered as indication of calculation instability or instability of tin oxide under the calculation conditions. The energetics of the reaction could be different if an alternative reaction path was found.

Based on our experimental studies SnO_2 is inferior catalyst to Ir and Ru oxides. In literature, it has been only used as partial replacement of Ir in Ir-Sn mixed oxides at small concentrations (Marshall et al., 2005 and 2007). SnO_2 catalyst was excluded from further binary catalyst studies.

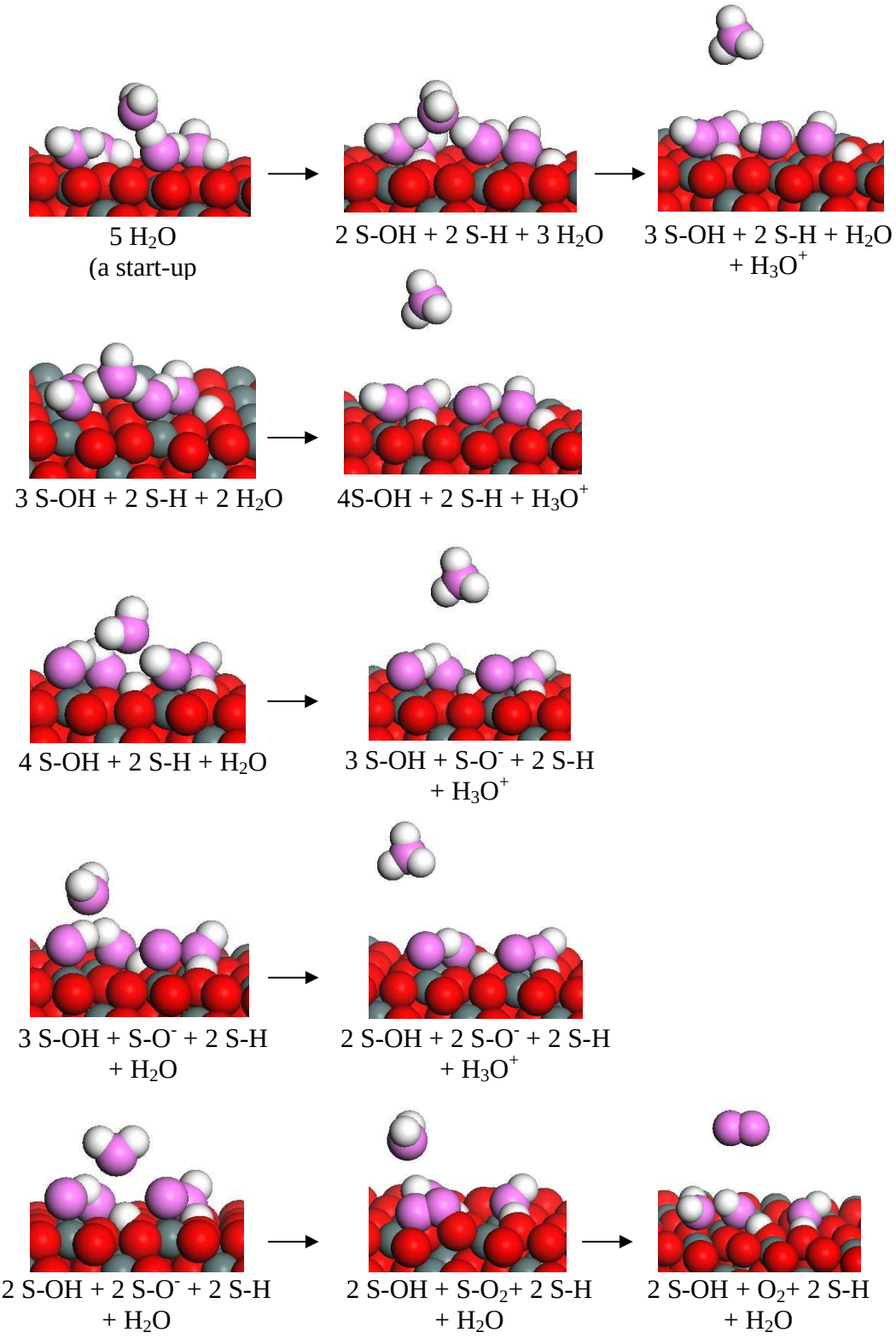

Figure 4. The reaction steps of the OER on the (001) surface of SnO_2.

Table 4 Energetics (eV) of the OER on the (001) surface of SnO_2.

	SnO_2		
	Barrier	Slope	Total
Step 1	Spontaneous sub reaction		
Step 2	1.26	0.02	1.28
Step 3	1.66	0.00	1.66
Step 4	0.49	0.75	1.24
Step 5	0.30	0.78	1.08
Step 6	0.17	-4.13	-3.96
Step 7	1.15	-1.52	-0.38
			0.92

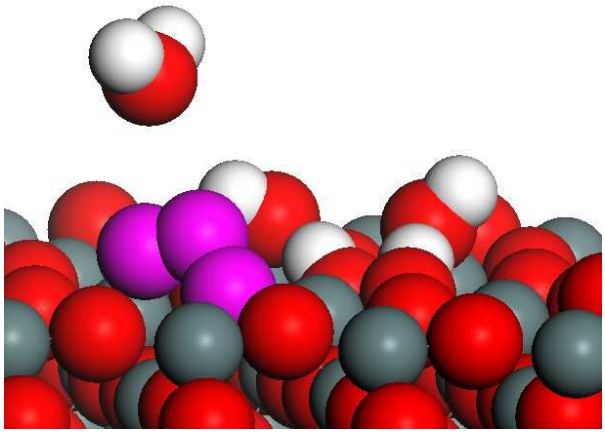

Figure 5. Step 6 of the OER where a trioxygen molecule forms as an intermediate product on the (001) surface of SnO_2.

8. Energetics on the stepped (101) and (201) surfaces

Based on the energetics of the calculated OER (Table 3), there are reaction steps, the barrier energies of which are rather high, over 4 eV. Therefore, in addition to the (001) surface, the stepped (101) surface and its multiple plane, the (201) surface, were also included into reaction mechanism studies in order to find out an energetically more favourable reaction path for the OER. Binary $RuIrO_4$ and tertiary Ir_2RuSnO_8 catalysts (Figure 2) were studied. The energetics are presented in Table 5. The reaction proceeds according to Scheme 2 on the $RuIrO_4$ surfaces. On the Ir_2RuSnO_8 surface, the reaction proceeds according to Scheme 3 around Ir and Sn atoms, but a trioxygen molecule does not appear on the surface unlike on the SnO_2 surface.

Table 5. Energetics (eV) of OER on the (001) and (101) surface of $RuIrO_4$, and the (201) surface of Ir_2RuSnO_8.

	$RuIrO_4$ (001)			**$RuIrO_4$ (101)**			**Ir_2RuSnO_8 (201)**		
	Barrier	Slope	Total	Barrier	Slope	Total	Barrier	Slope	Total
Step 1	0.87	-0.20	0.67	2.23	-0.96	1.27	-0.28	-1.83	-2.11
Step 2	0.48	-0.09	0.39	0.73	-3.01	-2.28	0.97	-2.60	-1.63
Step 3	0.65	-0.34	0.31	1.33	-2.14	-0.81	0.96	1.25	-0.29
Step 4	0.65	-0.10	0.55	0.88	-1.95	-1.07	1.05	1.39	-0.34
Step 5	4.55	-3.11	1.44	0.68	-0.25	0.38	5.60	-5.46	0.14
Step 6	2.17	-1.19	0.98	4.54	-2.50	2.04	1.09	1.59	-0.50
Step 7	5.39	-4.58	0.81	4.54	-5.15	-0.61	2.93	-1.14	1.79
			5.15			-1.08			-2.94

Comparison of the energetics of the OER on the (001) and (101) surfaces of $RuIrO_4$ (Table 5) reveals that the desorption of protons becomes exothermic reaction on the $RuIrO_4$ (101) surface although the barrier values are higher than on the (001) surface (Steps 2-4 and Step 7). This calculated exothermic desorption of protons could be indication of spontaneous reaction on the positively charged surface. On the other hand, the total energy needed for the formation and desorption of oxygen (Steps 5 and 6) is the same, 2.42 eV, on the (001) and (101) surfaces. Step 6, the desorption of the surface oxygen molecule, becomes the RDS on the (101) surface. Also, the barrier energies for the RDS are almost the same (4.55 eV and 4.54 eV) in the case of $RuIrO_4$ although the steps are different. If the barrier energy of the RDS is determining the catalyst activity, there is not much difference in the activity of the (001) and (101) surfaces of $RuIrO_4$. The effect of increased surface area due to the steps on the (101) surface for the activity of the $RuIrO_4$ is assumed minor, because the ratio of the stepped surfaces of the catalyst surface area is under 0.04% according to the BFDH (Bravais-Friedel Donnay-Harker) estimation method.

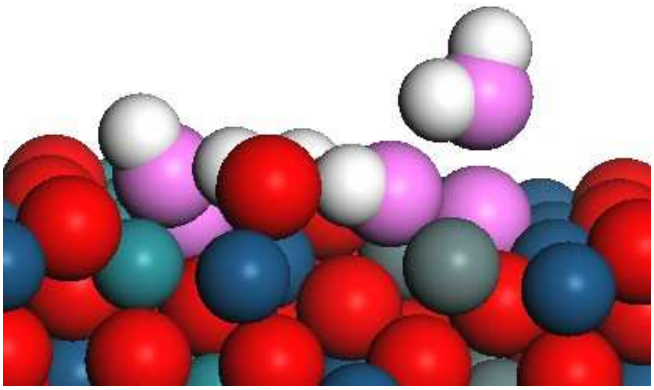

Figure 6. Step 5 of the OER on the (201) surface of Ir_2RuSnO_8.

The (201) surface of the tertiary Ir_2RuSnO_8 catalyst (Figure 2b) is flexible compared to the (101) surface of the $RuIrO_4$ (Figure 2a). This means that the positions of the surface atoms vary significantly during surface reactions, and the flexible surface structure can promote the reactions. The energy values in Table 5 indicate that the dissociation of water is strongly exothermic reaction, but only $^2/_5$ of water molecules dissociate in this first step. Dissociation of water continues during the desorption of protons from the surface. The desorption of protons is mainly exothermic reaction, but the energy barrier for the desorption of the fourth proton (Step 5 of Scheme 3) is 5.60 eV. The energy is needed to break hydrogen bonding between surface hydroxyl groups (Figure 6). Further, it is possible that the reaction can proceed after this RDS via other reaction paths, but these possibilities have not been studied.

Experimental studies carried out by us or reported in literature (Marshall et al. 2007) have not shown any promotional effect of Sn on Ir-Ru mixed oxides. The barrier energy of the calculated RDS of 5.60 eV is higher than for the other calculated surfaces.

The formation and desorption of an oxygen molecule from the Ir_2RuSnO_8 surface demands only 1.29 eV. This is much less than on the $RuIrO_4$ surfaces.

9. Discussion

Our modelling approach is showing surface oxygen molecule S-O_2 as reaction intermediate or transition state and not the peroxide S-OOH (= HOO*) as in the literature references. The study was performed on an adsorbate free surface and only five water molecules were available for the reaction. It could be more realistic to assume that the positively charged surface is at least partially covered by hydroxides S-OH. Moreover, positive barrier energies are reported for surface proton desorption even on the positively charged surface which appears not physical at first sight. This effect could, however, be attributed to surface charge density distribution on the surfaces and in the case of Ir_2RuSnO_8 to additional hydrogen bonding of the protons to surface hydroxyl groups.

The modelling results on the planar (001) surface would indicate that IrO_2 is more active towards oxygen evolution than RuO_2 if the formation of the S-O_2 were the RDS. This is in contradiction to experimental data on planar surfaces (Koetz and Stucki, 1986) and electrochemical surface area (ECSA) corrected data on Ir and Ru oxide nanoparticles (Mattos-Costa et al., 1998; Marshall et al., 2007). The model indicates that the reaction mechanism on IrO_2 and RuO_2 surfaces would be the same. However, it has been claimed that oxygen evolves on Ir in valence state VI i.e. IrO_3 and on Ru in valence state VII i.e. RuO_4 (Koetz and Stucki, 1986). These higher oxides could not be accounted for by our model.

The modelling results on the (001) and (101) surfaces give qualitative insight to the experimentally observed synergetic effects of Ir and Ru on the mixed oxide surfaces. However, real quantitative results have not been obtained.

It is difficult to correlate the surface charge to electrochemical potential. In this respect, the approach taken by Rossmeisl et al. (Rossmeisl et al., 2007) appears to be more appropriate. They were also able to reproduce the famous volcano curve from Trasatti (Trasatti, 1984). However, even their model is limited to low polarization over potentials. Experimental data (Trasatti, 1984; Xu et al., 2011) shows clearly two distinct Tafel slopes below and above about 1.5 V (RHE) which is an indication of change of reaction mechanisms. At high potentials the mechanism is becoming diffusion controlled which further complicates the analysis of the surface reaction steps.

As a summary, it can be said that the calculated OER on different catalyst surfaces gives trends of superiorities of catalysts. However, the exact catalyst composition cannot be defined yet according to these calculated results. Molecular modelling can be used to explain the functionality of the catalysts in the OER, but our approach is not suited as a rapid screening method for developing and selecting promising catalyst material compositions.

References

Accelrys, 2009, *MS Modeling*, Release 5.0. San Diego: Accelrys Software Inc.

Bockris J. O'M, 1956, Kinetics of Activation Controlled Consecutive Electrochemical Reactions: Anodic Evolution of Oxygen, *J. Chem. Phys.* 24, pp. 817-827.

Koetz R. and Stucki S., 1986, Stabilization of RuO_2 by IrO_2 for anodic oxygen evolution in acid media, *Electrochim. Acta* 31, pp. 1311-1316.

Marshall A., Børresen B., Hagen G., Tsypkin M. and Tunold R., 2007, Electrochemical characterisation of $Ir_xSn_{1-x}O_2$ powders as oxygen evolution electrocatalysts, *Electrochimica Acta* 51 pp. 3161–3167.

Marshall A., Børresen B., Hagen G., Tsypkin M. and Tunold R., 2007, Hydrogen production by advanced proton exchange membrane (PEM) water electrolysers—Reduced energy consumption by improved electrocatalysis, *Energy* 32, pp. 431–436.

Mattos-Costa F.I., de Lima-Neto P., Machadoa S.A.S. and Avac L.A., 1998, Characterisation of surfaces modifed by sol-gel derived $Ru_xIr_{1-x}O_2$ coatings for oxygen evolution in acid medium, *Electrochimica Acta* 44, pp. 1515-1523.

Rossmeisl, J., Logadottir, A., and Nørskov, J. K., 2005, Electrolysis of water on (oxidized) metal surfaces, *Chem. Phys*., Vol. 319, pp. 178-184.

Rossmeisl, J., Qu, Z.-W., Zhu, H., Kroes, G.-J., and Nørskov, J. K., 2007, Electrolysis of water on oxide surfaces, *J. Electroanal. Chem.*, Vol. 607, pp. 83-89.

Trasatti S., 1984, Electrocatalysis in the anodic evolution of oxygen and chlorine, *Electrochimica Acta* 29, No 14, pp. 1503-1512.

Xu J., Wanga M., Liua G., Li J. and Wang X, 2011, The physical–chemical properties and electrocatalytic performance of iridium oxide in oxygen evolution, *Electrochimica Acta* 56, pp. 10223–10230.